

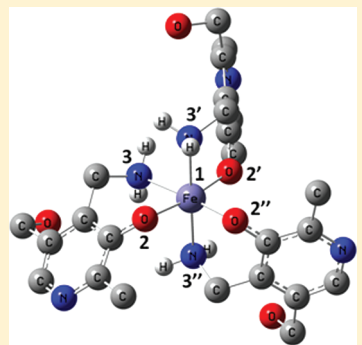
High- and Low-Spin Fe(III) Complexes of Various AGE Inhibitors

J. Ortega-Castro, J. Frau, R. Casasnovas, D. Fernández, J. Donoso, and F. Muñoz*

Institut d'Investigació en Ciències de la Salut (IUNICS), Departament de Química, Universitat de les Illes Balears, E-07122 Palma de Mallorca, Spain

S Supporting Information

ABSTRACT: Density functional theory calculations [CPCM/UM06/6-31+G(d,p)] were used to elucidate the structures and relative stability of Fe(III) complexes with various ligands that inhibit the formation of advanced glycation end products (AGEs) or iron overloaded disease (viz. aminoguanidine, pyridoxamine, LR-74, Amadori compounds, and ascorbic acid). EDTA was used as the free energy reference ligand. The distorted neutral octahedral complex containing one iron atom and three molecules of pyridoxamine [$\text{Fe}(\text{PM})_3$] was found to be the most stable. The stability of the complexes decreases in the following chelate sequence: pyridoxamine, Amadori complex, aminoguanidine, LR inhibitor, and ascorbic acid.



INTRODUCTION

Iron is essential for life. In fact, it plays a major role in many cellular processes including energy production, oxygen transport, and DNA synthesis.^{1–3} Also, it acts as a cofactor for a number of enzymes. Its catalytic activity stems from its redox properties; thus, iron can alternate between two oxidation states [Fe(II) and Fe(III)], which allows it to act as an electron acceptor or donor. However, the presence of excessive amounts of iron has been associated with age-related neurodegenerations such as age-related macular degeneration,⁴ Alzheimer's disease,⁵ and Parkinson's disease.⁶ In fact, Fe excess is toxic because it can cause the formation of reactive oxygen species (ROS), leading to potential tissue damage^{7,8} and also of reactive carbonyl species (RCS). The biological significance of iron and its role in some diseases are both a result of its involvement in redox processes.²

Although iron can be metabolized by a large number of proteins, no efficient excretion mechanisms seemingly exist to correct an excess of this element. Iron overload can be the result of (1) increased dietary absorption of the metal, (2) parenteral administration in transfusions and (3) pathological conditions (particularly of the brain).⁹ Local accumulation of Fe(III) is closely related to pathological lesions such as senile plaques, neurofibrillary tangles, and neuropil threads in patients with Alzheimer's disease.⁵ This has fostered the clinical use of chelating compounds to absorb Fe excess and protect patients from its deleterious effects. Also, there has been much research into the effectiveness of Fe complexes as anticancer agents.¹⁰

Iron chelation therapy involves the use of ligands to bind iron to prevent potentially fatal conditions such as iron overload disease or cancer.¹⁰ The earliest chelates used to capture Fe(III) for this purpose were similar to siderophores, which are low-molecular weight compounds capable of binding Fe(III) in its insoluble state as desferrioxamine (DFO) in the

same way as streptomyces and nocardia microbes. However, this compound has some contraindications that make it unsuitable for use in humans.^{9–11} Also, many ligands capable of retaining Fe(II) more effectively have a greater affinity for other biologically significant divalent metals including Cu(II) and Zn(II). This makes finding a harmless, selective ligand for Fe(II) an extremely difficult task. A number of trivalent cations such as Al(III) and Ga(III) are not essential for cell life, and, in practice, Fe(III) is a better chelating target under biological conditions.⁹

ROS and RCS can come from other sources including Maillard reaction or glycation,¹² which is a spontaneous nonenzymatic aminocarbonyl glycation reaction between reducing sugars and proteins or lipids. The process initially involves the reversible condensation of a terminal amino group in a protein or amino-phospholipid with a carbonyl group in the sugar to yield a Schiff base. The Schiff base is unstable and can undergo Amadori rearrangement to form the α -amino ketone. This Amadori compound can next form advanced glycation end products (AGEs) and advanced lipoxidation end products (ALEs), which can cause not only deterioration of tissues and organs related to normal aging but also some medical conditions such as diabetes, atherosclerosis, and chronic inflammatory diseases.^{13–17}

AGE inhibitors are believed to act by scavenging carbonyl and radical species, and also to inhibit the oxidation of Amadori compounds by chelating metal ions such as Cu(II) and Fe(III), which catalyze their autoxidation.¹² However, AGE inhibition is seemingly the primary result of metal chelation rather than carbonyl trapping activity.^{18–21} A knowledge of the chelating

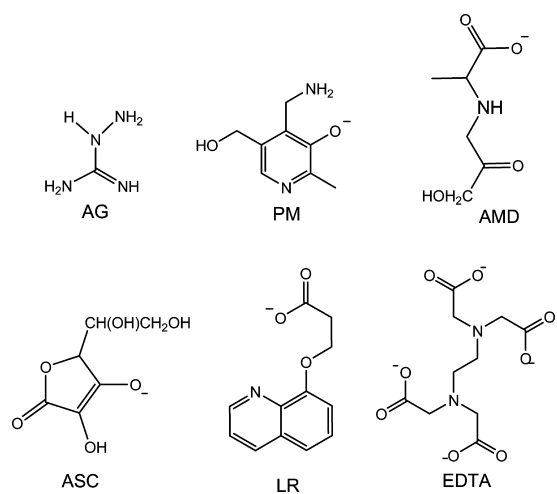
Received: October 24, 2011

Revised: February 24, 2012

Published: February 27, 2012

properties of AGE inhibitors is essential with a view to understanding the mechanism of action of some drugs and the potential benefits of chelation therapy against diabetes and chronic inflammatory diseases.¹⁹ Aminoguanidine (AG in Scheme 1) and various other compounds have shown promise

Scheme 1. Structure of Aminoguanidine (AG), Pyridoxamine (PM), Amadori Compound (AMD), Ascorbic Acid (ASC), LR74 (LR), and EDTA



for the treatment of diabetes complications. Aminoguanidine chelates catalytic metal ions and inhibits the oxidation of other compounds. However, it does not inhibit the formation of post-Amadori AGEs. On the other hand, pyridoxamine (PM, Scheme 1) chelates catalytic metal ions and inhibits the oxidation of certain compounds and the formation of post-Amadori AGEs.^{19–21} New aromatic compounds such as LR-74 exhibit potent AGE inhibitory action. Although their mechanisms of action of these compounds are unclear, there is some evidence that chelation of transition metals and/or trapping or indirect inhibition of the formation of reactive carbonyl compounds play some role in them.¹⁹

Our group has used ¹³C NMR to experimentally determine the equilibrium formation constants for Zn(II) complexes of pyridoxamine, aminoguanidine, and ascorbic acid.¹⁸ Also, the formation of Schiff bases of a pyridoxamine analogue with two different aldehydes has been examined on theoretical grounds.²² Other computational studies on known inhibitors including pyridoxamine and aminoguanidine,²³ and a new inhibitor named LR-74,^{19,24} have also been reported. The theoretical calculations provide a powerful means for elucidating structural and energy-related properties of metal complexes.^{25–30}

In this work, we used theoretical calculations to study the formation of Fe(III) complexes by aminoguanidine (AG), pyridoxamine (PM), a model Amadori compound model (AMD), LR-74 (LR), ascorbic acid (ASC), and EDTA (Scheme 1). The geometric properties, stability and biological significance of the complexes are discussed. The most important complexes were additionally subjected to charge density analysis (QTAIM).³¹

MATERIALS AND METHODS

DFT calculations were performed with the Gaussian09 software package.³² All structures were fully optimized at the UM06/6-

31+G(d,p)^{33,34} and UB3LYP/6-31+G(d)³⁵ levels of theory, using the COSMO polarizable continuum model (CPCM)^{36,37} to mimic the water solvent effect. B3LYP is a hybrid functional used widely in the literature and M06 is a new hybrid meta functional recently proposed by Zhao and Truhlar and recommended for application in organometallic and inorganic-metallic chemistry.^{33,34} Each optimized structure was subjected to vibrational analysis to calculate its free energy and characterize it as an energy minimum. All structures had positive-only force constants.

We modeled the EDTA-Fe complex (a well-known and highly stable complex) as a reference for the complexes of the studied AGE inhibitors. The free energy of this complex is -169.7 and -173.2 kcal/mol at M07 and B3LYP levels, respectively.

High-spin Fe(III) is a hard Lewis acid by virtue of its high positive charge density. The most stable bonds formed by this cation are with hard ligands such as charged oxygen atoms. On the other hand, Fe(II), which has a relatively low charge density, is preferentially complexed by chelates containing weak electron donor atoms such as nitrogen.³⁸ An extensive search in the databases of the Cambridge Crystallographic Data Centre³⁹ revealed that most iron complexes exhibit octahedral geometries. The multiplicity of compounds with high nitrogen content is determined by the nature of the ligands attached to iron and results from competition between ligand field splitting and spin pairing energy. Ferric iron has 3d electrons and can thus adopt $S = 1/2$ or $S = 5/2$ configurations. When the ligand field splitting is small, electron pairing dominates and a high-spin configuration results. Conversely, a low-spin configuration is preferentially adopted with strong-field ligands such as CN^- , *o*-phenanthroline, histidine, or *o,o'*-bipyridine.^{38,40} Most of these chelates exhibit octahedral coordination. Only the aminoguanidine (AG-3s), pyridoxamine (PM-3s), and Amadori (AMD-3s) complexes among those studied here could be low-spin complexes.

Chelate topology was the subject of a comprehensive study involving the use of the software AIMall⁴¹ with the wave function calculated at the CPCM/UM06/6-31+G(d,p) level. In this work, we focused on metal-ligand bonding. The specific parameters calculated here were the bond critical point (BCP), ring critical point (RCP), and electron density ($\rho(\mathbf{r}_c)$) and the Laplacian of the electron density ($\nabla^2\rho(\mathbf{r}_c)$) at the BCP. Supporting Information including the distance from the Fe atom to the BCP ($d_{\text{Fe}-\text{BCP}}$), that of N or O to the BCP ($d_{\text{BCP-X}}$), the three eigenvalues of the Hessian matrix (λ_1 , λ_2 and λ_3), and ellipticity is also provided.

RESULTS AND DISCUSSION

1. Aminoguanidine Complexes. The coordination chemistry of aminoguanidine with some transition metals has been studied and elucidated for some complexes such as the square-planar double chelate $[\text{Cu}(\text{AG})_2](\text{NO}_3)_2$.^{42,43} Similar structures have been identified for complexes with Pd or Pt as central cation.^{44,45} In a recent theoretical study, our research group found that a square-planar complex ($[\text{Cu}(\text{AG})_2]^{2+}$) was the most stable of the aminoguanidine complexes studied.²³

In this work, we studied the Fe(III) complexes AG-1s $\{[\text{Fe}(\text{AG})_2]^{3+}\}$; AG-2s $\{[\text{Fe}(\text{AG})_2(\text{H}_2\text{O})_2]^{3+}\}$, and AG-3s $\{[\text{Fe}(\text{AG})_3]^{3+}\}$. They are high spin except AG-3s that was studied in high and low spin. Aminoguanidine is an unsymmetric bidentate ligand that coordinates through its terminal hydrazine N2 atom and its imine N3 atom. The

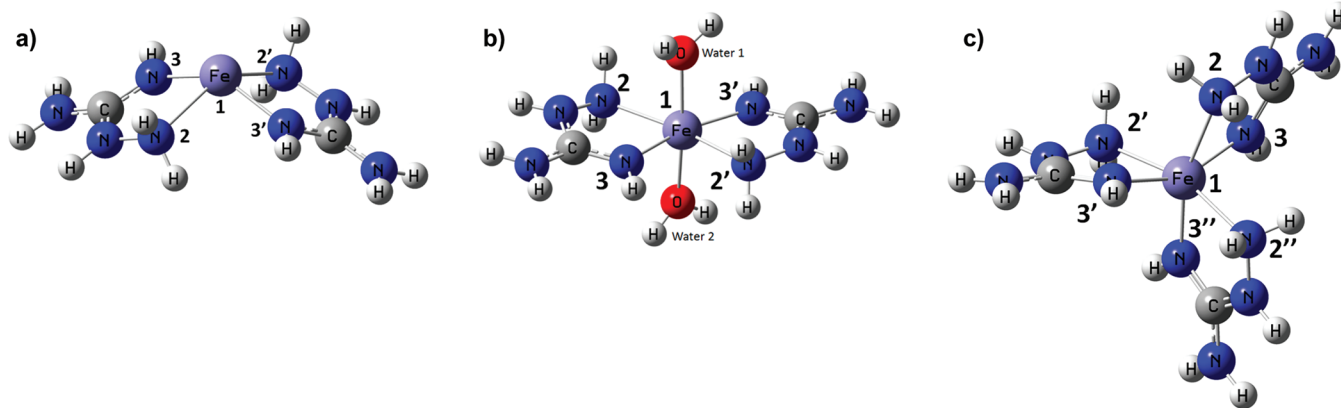


Figure 1. Structures of the AG-1s complex ($[\text{Fe}(\text{AG})_2]^{3+}$) (1A), AG-2s complex ($[\text{Fe}(\text{AG})_2(\text{H}_2\text{O})_2]^{3+}$) (1B), and AG-3s complex ($[\text{Fe}(\text{AG})_3]^{3+}$) (1C).

aminoguanidine ligand is neutral. Parts A–C of Figure 1 show the structures of the high-spin Fe(III)–aminoguanidine complexes studied, and Table 1 lists the relevant geometric and energy-related parameters of the most stable complexes.

The solvation complex AG-1s exhibited a distorted square-planar geometry; thus, the iron atom fell outside the plane formed by the hydrazine and imine nitrogens in the aminoguanidine molecule (Figure 1A). The AG-2s complex (Figure 1B) exhibited an also distorted octahedral structure where the low bite angle (φ) of aminoguanidine (N2–Fe1–N3) constrained the five-member ring between the metal and ligand to 76.4° , which differs considerably from the straight angle ($\varphi = 90^\circ$) in the ideal structure. Similar results have been reported for complexes former with other central cations ($[\text{X}(\text{AG})_2]^{2+}$, with $\text{X} = \text{Cu}^{2+}$, Pd^{2+} , or Pt^{2+}).⁴⁴

Unlike AG-1s and AG-2s, which contained two trans-oriented bidentate aminoguanidines ligands, AG-3s had three AG bidentate ligands forming a distorted octahedral structure (Figure 1C). The presence of three aminoguanidine molecules reduces the bite angle. One of the factors distorting the octahedral geometry is the presence of bidentate ligands.

As can be seen, the bond distance of the amine nitrogen (Fe1–N3) was much shorter than Fe1–N2, Fe1–Ow1, and Fe1–Ow2, which testifies to the increased chelating power of the guanidine nitrogen and is consistent with previous results for complexes of other central cations.^{44,46}

All free energy values were negative, so the chelation reactions were highly exothermic. On the basis of the ΔG values obtained (Table 1), the high-spin octahedral complex AG-3s was the most stable. Also, on the basis of the ligand field theory, low-spin complexes with high nitrogen content (e.g., AG) are more energetically favorable than high-spin complexes. We failed to detect this pattern with the M06 functional but observed a small energy difference in favor of the low-spin complex with the B3LYP functional.

In this work, we modeled such a well-known and highly stable complex as EDTA–Fe for use as an energy reference. The free energy of this complex as determined at the CPCM/M06/6-31+G(d,p) level, $\Delta G = -169.7$ kcal/mol, is approximately 50 kcal/mol lower than those for the aminoguanidine complexes. The EDTA–Fe complex has a distorted octahedral geometry and average Fe–N and Fe–O distances differing by less than 2.5% from their experimental counterparts.⁴⁷ Also, it has 5 five-membered rings with an average bite angle of 78.5° .

(experimental value 75.0°), which is slightly higher than that for AG-3s.

2. Pyridoxamine Complexes. We studied the tetrahedral complex PM-1s ($[\text{Fe}(\text{PM})_2]^+$) and the octahedral complex PM-2s ($[\text{Fe}(\text{PM})_2(\text{H}_2\text{O})_2]^+$) and PM-3s ($[\text{Fe}(\text{PM})_3]$). The pyridoxamine monoanion was assumed to have its amine and pyridine nitrogens in unprotonated form, and the phenol oxygen in deprotonated form, throughout.⁴⁸ PM-1s and PM-2s contained two trans-oriented bidentate pyridoxamine molecules. On the other hand, PM-3s was geometrically arranged, which allowed the formation of an octahedral complex. The unsymmetric ligands coordinated a six-membered ring with the central cation via the amine N and the phenolate group. In all complexes, the Fe1–O2 distance was considerably shorter than the Fe1–N3 distance, which confirms the increased chelating power of the phenolic oxygen (Table 2, Figure 2A–C). A similar trend was experimentally observed in high-spin Fe(III) pyridoxal thiosemicarbazone complexes^{49,50} and Cu(II) complexes.^{51–54}

PM-1s had a distorted tetrahedral geometry (Figure 2A, Table 2). The formation of a distorted octahedral complex with two pyridoxamines in the same plane and two water molecules in axial positions is not sufficient to provide stability to the new complex formed (PM-2s); in fact, it had a smaller ΔG value than PM-1s. The neutral complex PM-3s consisted of three pyridoxamine molecules bonded to the central cation (Figure 2C). The presence of three bidentate ligands increased the bond distances between the metal and the ligands. The six-membered metallacycles of PM-3s were planar and located in three interperpendicular planes, the corresponding bite angles (φ) for each ligand being 85.2° , 89.0° , and 88.3° . Like the previous complexes, and in general form, they exhibited no Jahn–Teller distortion. A comparison of high- and low-spin PM-3s revealed that the Fe1–N3 bond distance was ca. 0.2 Å shorter and φ approximately 4.5° lower in the low-spin complex, all other parameters being virtually identical for the two complexes. The neutral high-spin chelate $[\text{Fe}(\text{PM})_3]$ was the most stable complex studied, except for EDTA–Fe. The increased size of the ring formed between the metal and ligand led to a less distorted octahedral geometry than in the other complexes.

Both functionals, M06 and B3LYP, predict that the high-spin PM complex is more stable than the low-spin one.

3. Amadori Compound Complexes. The formation of Cu(II) and Fe(III) complexes with Amadori compounds is

Table 1. Main Geometric and Energetic Parameters of the Fe^{3+} –Aminoguanidine Complexes in Solution with M06/6-31+G(d,p) and B3LYP/6-31+G(d) Functional (Distances in Å and Angles in deg)

	AG-1s (h.s.)		AG-2s (h.s.)		AG-3s (h.s.)		AG3s (l.s.)	
	M06	B3LYP	M06	B3LYP	M06	B3LYP	M06	B3LYP
Fe1-N2	2.220/2.220 ^a	2.230/2.230 ^a	2.235/2.187 ^a	2.223/2.222 ^a	2.298/2.223/2.238 ^b	2.329/2.249/2.271 ^b	2.062/2.006/2.014 ^b	2.070/2.025/2.029 ^b
Fe1-N3	1.952/1.952 ^c	1.949/1.949 ^c	1.993/1.973 ^c	1.992/1.989 ^c	1.982/2.011/1.997 ^d	1.995/2.024/2.012 ^d	1.952/1.899/1.878 ^d	1.949/1.917/1.893 ^d
Fe1-Ow1			2.102	2.112				
Fe1-Ow2			2.071	2.114				
N2-Fe1-N3 (ρ)	76.4/76.4 ^e	77.0/77.0 ^e	76.3/77.5 ^e	77.1/77.0 ^e	74.5/75.6/76.1 ^f	73.6/75.1/75.2 ^f	78.8/82.1/82.6 ^f	78.6/80.6/82.1 ^f
N3-Fe1-Ow1			89.9/90.8 ^g	90.0/90.0 ^g				
N2-Fe1-Ow2			94.7/90.2 ^h	87.0/92.5 ^h				
N2-Fe1-N3'	89.7	101.2	87.0	103.6	85.6/90.6/99.7 ⁱ	85.5/90.0/100.8 ⁱ	90.5/91.9/90.7 ⁱ	90.5/90.9/92.1 ⁱ
N3-Fe1-N2'	89.7	101.2	119.1	102.3	93.6/96.3/162.0 ^j	94.1/96.4/160.8 ^j	92.5/95.7/170.6 ^j	91.8/96.8/170.2 ^j
ΔG^k (kcal/mol)	-72.0	-85.0	-78.8	-80.1	-114.9	-115.3	-96.6	-116.4

Table 2. Main Geometric and Energetic Parameters of the Fe^{3+} -Pvridoxamine Complexes in Solution (Distances in Å and Angles in deg)

	PM-1s (h.s.)		PM-2s (h.s.)		PM-3s (h.s.)		PM-3s (l.s.)	
	M06	B3LYP	M06	B3LYP	M06	B3LYP	M06	B3LYP
Fe1–O2	1.84/ ^a 1.845 ^a	1.880/ ^a 1.882 ^a	1.896/ ^a 1.897 ^a	1.901/ ^a 1.901 ^a	1.946/ ^b 1.932/ ^b 1.963 ^b	1.943/ ^b 1.945/ ^b 1.979 ^b	1.920/ ^b 1.904/ ^b 1.893 ^b	1.919/ ^b 1.913/ ^b 1.896 ^b
Fe1–N3	2.080/ ^c 2.088 ^c	2.170/ ^c 2.170 ^c	2.163/ ^c 2.163 ^c	2.178/ ^c 2.178 ^c	2.267/ ^d 2.193/ ^d 2.182 ^d	2.288/ ^d 2.209/ ^d 2.209 ^d	2.036/ ^d 2.011/ ^d 2.003 ^d	2.045/ ^d 2.017/ ^d 2.014 ^d
Fe1–Owl			2.131	2.174				
Fe1–Ow2			2.131	2.174				
O2–Fe–N3 (ϕ)	93.1/ ^e 94.5 ^e	87.6/ ^e 87.6 ^e	89.3/ ^e 89.3 ^e	87.6/ ^e 87.7 ^e	85.2/ ^f 89.0/ ^f 88.3 ^f	83.3/ ^f 87.4/ ^f 86.7 ^f	94.1/ ^f 89.9/ ^f 93.0 ^f	89.4/ ^f 92.5/ ^f 92.7 ^f
O2–Fe–Owl			89.7/ ^g 90.3 ^g	89.6/ ^g 90.4 ^g				
O2–Fe–Ow2			90.3/ ^h 89.7 ^h	90.3/ ^h 89.6 ^h				
N3–Fe–Owl			88.0/ ⁱ 92.0 ⁱ	92.4/ ⁱ 87.6 ⁱ				
N3–Fe–Ow2			92.0/ ^j 88.0 ^j	87.7/ ^j 92.3 ^j				
ΔG^k (kcal/mol)	-121.2	-124.3	-119.7	-120.8	-158.1	-154.5	-130.3	-147.8

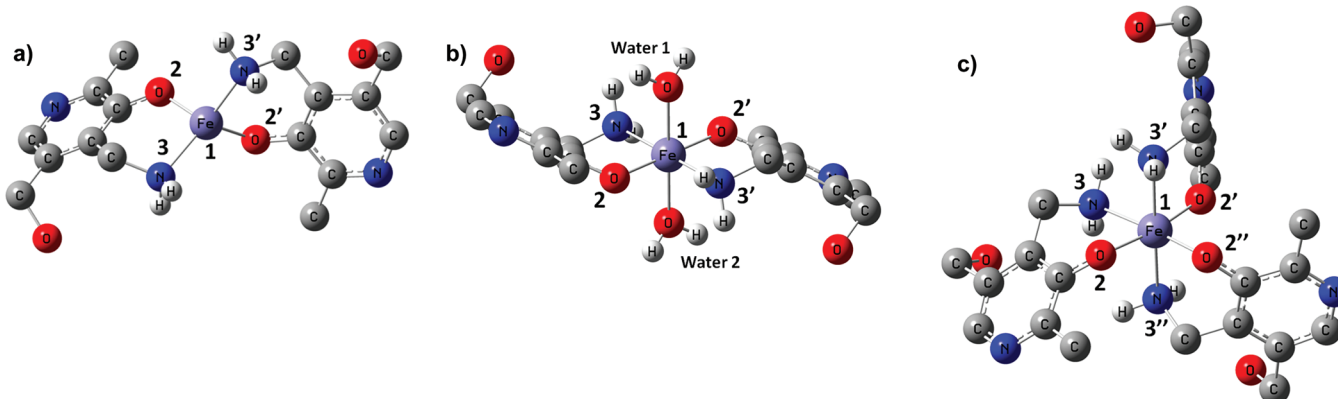


Figure 2. Structures of the PM-1s complex ($[Fe(PM)_2]^+$) (2A), PM-2s complex ($[Fe(PM)(H_2O)_2]^+$) (2B), and PM-3s complex ($[Fe(PM)_3]$) (2C). To clarify the structure, some hydrogen atoms of pyridoxamine have been removed.

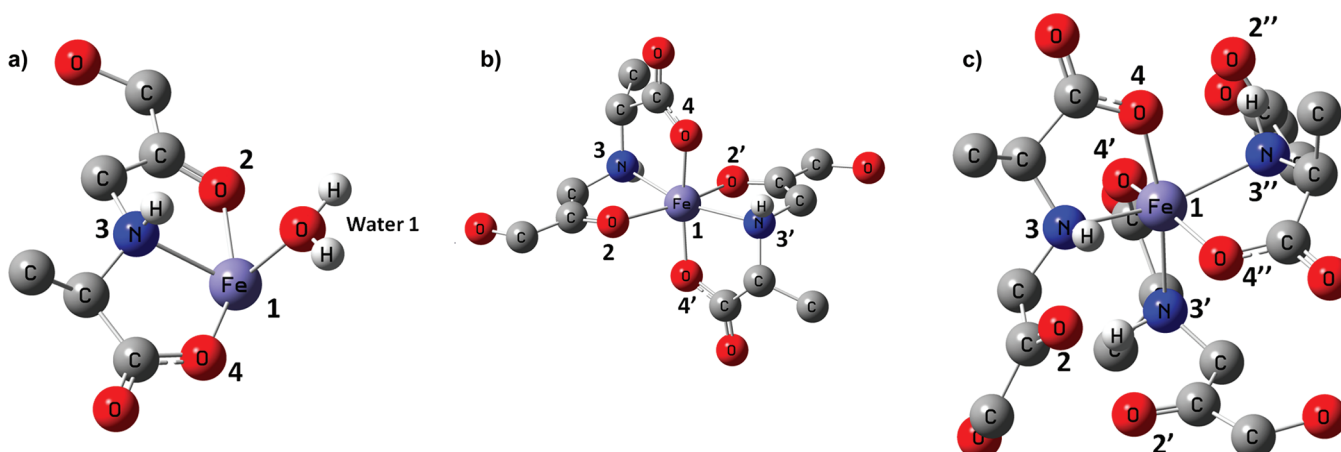


Figure 3. Structures of the AMD-1s complex ($[Fe(AMD)(H_2O)]^{2+}$) (3A), AMD-2s complex ($[Fe(AMD)_2]^+$) (3B), and AMD-3s complex ($[Fe(AMD)_3]$) (3C). To clarify the structure, some hydrogen atoms of the Amadori compound have been removed.

Table 3. Main Geometric and Energetic Parameters of the Fe^{3+} –Amadori Compound Complexes in Solution (Distances in Å and Angles in deg)

	AMD-1s (h.s.)		AMD-2s (h.s.)		AMD3s (h.s.)		AMD3s (l.s.)	
	M06	B3LYP	M06	B3LYP	M06	B3LYP	M06	B3LYP
Fe1–O2	2.030	2.043	2.119/2.106 ^a	2.124/2.116 ^a				
Fe1–N3	2.180	2.209	2.158/2.193 ^b	2.175/2.209 ^b	2.186/2.277/2.215 ^c	2.318/2.374/2.312 ^c	2.034/2.052/2.036 ^c	2.086/2.083/2.063 ^c
Fe1–O4	1.845	1.851	1.925/1.904 ^d	1.931/1.922 ^d	1.958/1.941/1.965 ^e	1.951/1.974/1.960 ^e	1.874/1.908/1.878 ^e	1.890/1.909/1.887 ^e
Fe1–Ow1	2.008	2.029						
O2–Fe–N3	76.1	76.0	76.4/77.9 ^f	76.7/78.1 ^f				
N3–Fe–O4 (φ)	78.2	77.9	83.3/80.6 ^g	82.9/79.9 ^g	77.1/75.9/79.1 ^h	74.1/73.1/76.3 ^h	82.7/81.4/85.4 ^h	81.2/81.4/83.9 ^h
O2–Fe–Ow1	89.0	89.0						
O4–Fe–Ow1	98.9	100.2						
ΔG^i (kcal/mol)	-49.1	-61.2	-100.7	-98.5	-126.1	-115.9	-96.6	-103.3

^aFe1–O2/Fe1–O2'. ^bFe1–N3/Fe1–N3'. ^cFe1–N3/Fe1–N3'/Fe1–N3". ^dFe1–O4/Fe1–O4'. ^eFe1–O4/Fe1–O4'/Fe1–O4". ^fO2–Fe–N3/O2'–Fe–N3'. ^gN3–Fe–O4/N3'–Fe–O4'. ^hN3–Fe–O4/N3'–Fe–O4'/N3"–Fe–O4". ⁱ $\Delta G = G(\text{complex}) + mG(\text{H}_2\text{O}) - G(\text{Fe}(\text{H}_2\text{O})_6^{3+}) - nG(\text{AMD})$.

believed to be one of the key steps in their degradation and the subsequent formation of AGEs.^{18–21} This has raised the need to carefully examine these complexes. In this work, we used a simplified model of the compound *N*-(1-deoxy-D-fructos-1-yl)-L-tryptophan obtained by partial removal of the sugar and the 1*H*-indole group as model compound (AMD).⁵⁵

The specific complexes examined included (1) AMD-1s $\{[Fe(AMD)(H_2O)]^{2+}\}$, a pseudotetrahedral complex containing a single molecule of Amadori compound as tridentate

ligand and one water molecule (Figure 3A); (2) AMD-2s ($[Fe(AMD)_2]^+$), where two molecules of Amadori compound acted as a tridentate ligand in a distorted octahedral complex (Figure 3B) and, as in the previous case, the ligand coordinated the central cation via the carboxyl oxygen atom, amino group and carbonyl oxygen of the sugar; and (3) AMD-3s ($[Fe(AMD)_3]$), where three AMD molecules formed a neutral complex by bonding exclusively via the carboxyl group and the amino nitrogen (Figure 3C). The acid group in the Amadori

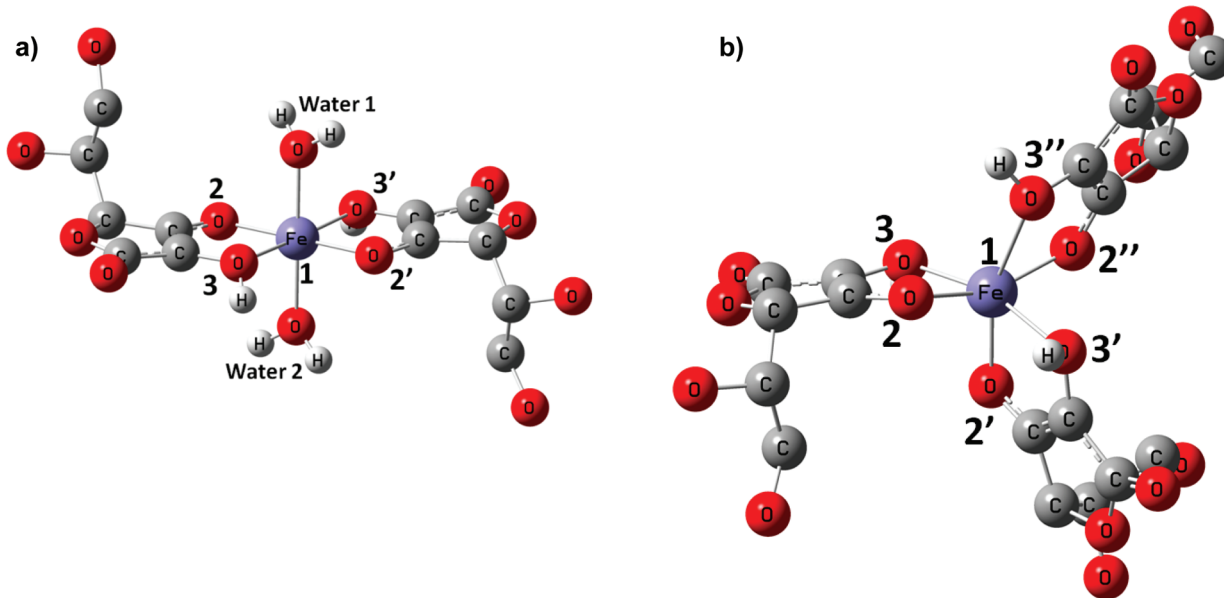


Figure 4. Structures of the ASC-1s complex ($[\text{Fe}(\text{ASC})_2(\text{H}_2\text{O})_2]^+$) (4A) and ASC-2s complex ($[\text{Fe}(\text{ASC})_3]$) (4B). To clarify the structure, some hydrogen atoms of Ascorbic acid have been removed.

Table 4. Main Geometric and Energetic Parameters of the Fe^{3+} –Ascorbic Acid Compound Complexes in Solution (Distances in Å and Angles in deg)

	ASC-1s (h.s.)		ASC-2s (h.s.)	
	M06	B3LYP	M06	B3LYP
Fe1–O2	1.930/1.934 ^a	1.869/1.878 ^a	1.939/1.938/1.890 ^b	1.954/1.953/1.870 ^b
Fe1–O3	2.193/2.187 ^c	3.596/3.581 ^c	2.214/2.253/2.488 ^d	2.323/2.351/4.510 ^d
Fe1–Ow1	2.067	2.068		
Fe1–Ow2	2.060	2.071		
O2–Fe–O3 (φ)	82.9/83.2 ^e	57.0/58.8 ^e	82.7/82.3/77.0 ^f	81.1/80.2/28.7 ^f
O3–Fe–Ow1	87.6/89.4 ^g	110.6/49.3 ^g		
O2–Fe–Ow1	89.4/90.0 ^h	98.8/104.7 ^h		
ΔG° (kcal/mol)	-52.7	-73.4	-77.0	-87.4

^aFe1–O2/Fe1–O2'. ^bFe1–O2/Fe1–O2'/Fe1–O2''. ^cFe1–O3/Fe1–O3'. ^dFe1–O3/Fe1–O3'/Fe1–O3''. ^eO2–Fe–O3/O2'–Fe–O3'. ^fO2–Fe–O3/O2'–Fe–O3'/O2''–Fe–O3''. ^gO3–Fe–Ow1/O3'–Fe–Ow1. ^hO2–Fe–Ow1/O2'–Fe–Ow1. ⁱ $\Delta G = G(\text{complex}) + mG(\text{H}_2\text{O}) - G(\text{Fe}(\text{H}_2\text{O})_6^{3+}) - nG(\text{ASC})$.

compound was assumed to be in deprotonated form in all cases.

The shortest distance in all complexes was that between the metal and the carboxyl oxygen (Fe1–O4), followed by that to the carbonyl oxygen (Fe1–O2) in those complexes where the Amadori compound acted as a tridentate ligand, and by the Fe1–N2 distance (Table 3). All complexes exhibited strong distortions from their ideal geometries. Also, AMD-3s was the most stable complex. These results are consistent with those of experimental studies of the formation of Cu(II), Pd(II), and Fe(III) complexes with an Amadori compound, which suggest that the compound acts only as a bidentate ligand and bonds to the metal via its carboxyl and amino group, but not through the carbonyl group in the sugar.^{56,57}

The most stable complex, AMD-3s, was studied in its high- and low-spin states (Table 3), which differed markedly in both geometry and energy. Thus, the high-spin state exhibited shorter metal–ligand distances and a higher bite angle, N3–Fe1–O4 (83.2° vs 77.4°), than the low-spin state. Although the low-spin complex was less markedly distorted than the high-spin complex, the latter was the most stable in the series of Amadori complexes in both functionals.

4. Ascorbic Acid Complexes. The coordination chemistry of ascorbic acid (vitamin C) has been extensively studied in response to the problems associated with its hydrolysis and redox reactions, and the instability of its complexes. In fact, virtually all complexes of ascorbate ion with transition metals form amorphous precipitates.⁵⁸ By exception, Unalerglu et al.⁵⁹ obtained a stable Cu(II)–ascorbate complex in non-aqueous solvents under anaerobic conditions.

Ascorbic acid is oxidized to a negligible extent by molecular oxygen in solutions containing low concentrations of heavy metal ions; the reaction, however, is considerably boosted by the presence of transition metals (especially Cu(II) and Fe(III)).^{60,61} The process involves one-electron steps and yields dehydroascorbate and hydrogen peroxide.⁶² Aqueous solutions containing Cu(II) and ascorbic acid equilibrate very rapidly, which suggests the formation of the chelate $[\text{Cu}(\text{ASC})]^+$. The dimeric complex $[\text{Cu}_2(\text{ASC})]^{2+}$ has also been suggested.^{59,63} Because the pK_a values for ascorbic acid are 4.2 and 11.6 (S8), ascorbate monoanion prevails at neutral pH. The monoanion is a bidentate ligand and binds the metal through the ascorbate ion O[−] and OH groups^{59,64} (Scheme 1).

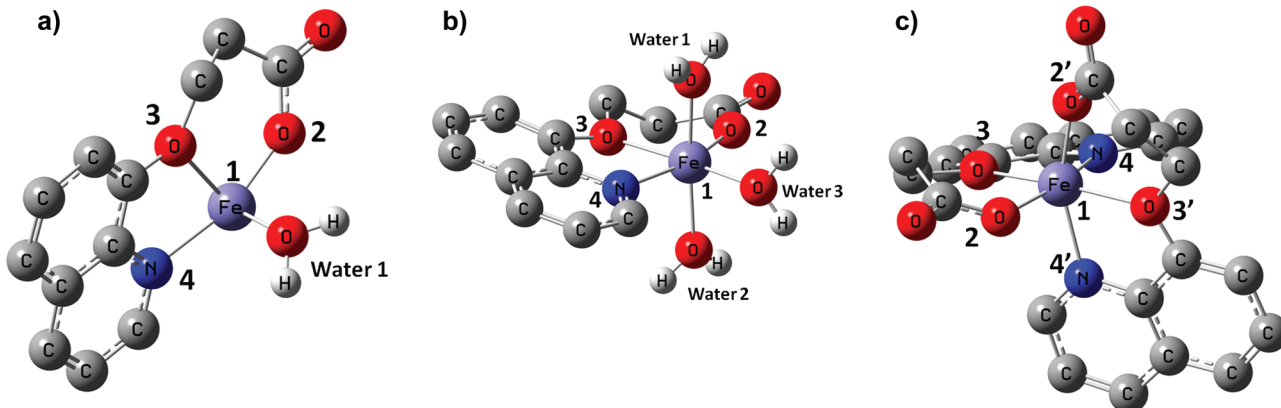


Figure 5. Structures of the LR-1s complex ($[\text{Fe}(\text{LR})(\text{H}_2\text{O})]^{2+}$) (5A), LR-2s complex ($[\text{Fe}(\text{LR})(\text{H}_2\text{O})_3]^{2+}$) (5B), and LR-3s complex ($[\text{Fe}(\text{LR})_2]^+$) (5C). To clarify the structure some hydrogen atoms of LR have been removed.

Table 5. Main Geometric and Energetic Parameters of the Fe^{3+} –LR-74 Compound Complexes in Solution (Distances in Å and Angles in deg)

	LR-1s (h.s.)		LR-2s (h.s.)		LR-3s (h. s.)	
	M06	B3LYP	M06	B3LYP	M06	B3LYP
Fe1–O2	1.813	1.824	1.838	1.842	1.890/1.892 ^a	1.886/1.896 ^a
Fe1–O3	2.103	2.147	2.153	2.183	2.162/2.162 ^b	2.321/2.279 ^b
Fe1–N4	2.049	2.065	2.069	2.086	2.128/2.128 ^c	2.135/2.171 ^c
Fe1–Ow1	2.038	2.085	2.064	2.091		
Fe1–Ow2			2.061	2.107		
Fe1–Ow3			2.050	2.082		
O2–Fe–O3 (φ_1)	87.5	86.8	86.9	86.1	84.8/84.8 ^d	84.5/82.4 ^d
O3–Fe–N4 (φ_2)	77.4	76.0	76.0	75.7	74.5/74.5 ^e	72.3/72.0 ^e
O2–Fe–Ow1	93.6	96.2	90.8	91.1		
N4–Fe–Ow1	92.9	94.1	88.5	88.9		
O3–Fe–Ow1	87.2	88.3	91.1	92.1		
O3–Fe–Ow2			96.7	99.6		
O3–Fe–Ow3			170.7	170.7		
ΔG^f (kcal/mol)	-49.5	-61.4	-59.7	-58.9	-104.3	-101.0

^aFe1–O2/Fe1–O2'. ^bFe1–O3/Fe1–O3'. ^cFe1–N4/Fe1–N4'. ^dO2–Fe–O3/O2'–Fe–O3'. ^eO3–Fe–N4/O3'–Fe–N4'. ^f $\Delta G = G(\text{complex}) + mG(\text{H}_2\text{O}) - G(\text{Fe}(\text{H}_2\text{O})_6^{3+}) - nG(\text{LR})$.

We examined the complexes ASC-1s $\{[\text{Fe}(\text{ASC})_2(\text{H}_2\text{O})_2]^+\}$ and ASC-2s $\{[\text{Fe}(\text{ASC})_3]\}$ (Figure 4, Table 4), of which ASC-2s was the more stable but was still 92.7 kcal/mol more unstable than the EDTA complex. Both complexes possessed a distorted octahedral structure when examined with the M06 functional (Figure 4, Table 4). With the B3LYP functional, however, ASC-1s possessed a pseudotetrahedral structure where ASC acted as a monodentate ligand via O^- in ascorbate ion. On the other hand, only one of the ligands in ASC-2s, which was pentacoordinated, was monodentate (see Supporting Information).

5. LR-74 Complexes. The LR-74 series included (1) LR-1s $\{[\text{Fe}(\text{LR-74})(\text{H}_2\text{O})]^{2+}\}$, a complex containing one LR-74 molecule as a tridentate ligand (viz. an amine group, an ether group, and a carboxyl group) and one water molecule; (2) LR-2s $\{[\text{Fe}(\text{LR-74})(\text{H}_2\text{O})_3]^{2+}\}$, a complex of nearly octahedral structure containing one LR-74 molecule and three water molecules; and (3) LR-3s $\{[\text{Fe}(\text{LR-74})_2]^+\}$, which consisted of two LR-74 molecules. The tridentate ligand LR possessed one six-membered and one five-membered metallacycles. Parts A–C of Figure 5 show the structures of the previous complexes, and Table 5 lists their most relevant geometric and energy-related parameters.

Overall, the Fe1–O2 distance was substantially shorter than the Fe1–O3 and Fe1–N4 distances, consistent with the increased chelating power of the carboxyl oxygen. On the other hand, the Fe–Ow1, Fe–Ow2, and Fe–Ow3 distances in LR-1s and LR-2s were similar to the Fe1–N4 distance. The presence of three explicit water molecules made the resulting complexes slightly more stable. However, the presence of two molecules of the ligand LR-74 led to the most stable compound in the series: LR-3s. The bite angle of LR was 84.8° in the six-membered ring (O2–Fe1–O3) and 74.5° in the five-membered ring (O3–Fe1–N4).

6. Analysis QTAIM. The studied complexes were subjected to a topological analysis under the QTAIM theory. The magnitude of the electron density at the bond critical point, $\rho(\mathbf{r}_c)$, was found to be directly correlated with bond distance and bond order. The Laplacian of the electron density exhibited charge concentration and depletion effects. When $\nabla^2\rho(\mathbf{r}_c) < 0$, the electron density is locally concentrated at \mathbf{r}_c , and when $\nabla^2\rho(\mathbf{r}_c) > 0$, it is locally depleted at \mathbf{r}_c . In addition, the Laplacian value at a (3,–1) bond critical point provides a description of the interaction between the bonded atoms as being closed-shell (ionic) or electron-shared (covalent). Bond ellipticity is a measure of π character in a bond. Table 6 shows detailed

Table 6. Topological Properties at the High-Spin Fe–X BCPs^a

		$\rho(r_c)$ (e Å ⁻³)	$\nabla^2\rho(r_c)$ (e Å ⁻⁵)	d_{Fe-X}	<i>b</i>		$\rho(r_c)$ (e Å ⁻³)	$\nabla^2\rho(r_c)$ (e Å ⁻⁵)	d_{Fe-X}	<i>b</i>	
EDTA	Fe1–O2	0.572	9.93	1.989	(1)	AMD-3s	Fe1–O4	0.603	11.05	1.951	(1)
	Fe1–O3	0.602	10.68	1.972	(1)		Fe1–O4'	0.644	11.97	1.974	(1)
	Fe1–O4	0.572	9.93	1.989	(1)		Fe1–O4"	0.613	10.94	1.960	(1)
	Fe1–O5	0.603	10.83	1.972	(1)		Fe1–N3	0.446	4.32	2.318	(5)
	Fe1–N6	0.389	3.66	2.242	(5)		Fe1–N3'	0.373	3.18	2.374	(5)
	Fe1–N7	0.389	3.66	2.242	(5)		Fe1–N3"	0.427	3.90	2.312	(5)
AG-3s	Fe1–N3	0.668	9.14	1.982	(2)	LR-3s	Fe1–O2	0.694	14.00	1.890	(1)
	Fe1–N3'	0.627	8.18	2.011	(2)		Fe1–O2'	0.694	14.00	1.892	(1)
	Fe1–N3"	0.650	8.41	1.997	(2)		Fe1–N4	0.488	5.36	2.162	(3)
	Fe1–N2	0.343	3.08	2.298	(5)		Fe1–N4'	0.488	5.34	2.162	(3)
	Fe1–N2'	0.402	3.93	2.233	(5)		Fe1–O3	0.360	5.21	2.128	(4)
	Fe1–N2"	0.389	3.77	2.238	(5)		Fe1–O3'	0.360	5.23	2.128	(4)
PM-3s	Fe1–O2	0.567	10.95	1.963	(1)	ASC-2s	Fe1–O2	0.665	11.94	1.939	(1)
	Fe1–O2"	0.593	11.62	1.946	(1)		Fe1–O2'	0.670	11.63	1.938	(1)
	Fe1–O2'	0.614	12.12	1.932	(1)		Fe1–O2"	0.738	14.38	1.890	(1)
	Fe1–N3	0.364	3.35	2.267	(5)		Fe1–O3	0.328	4.19	2.214	(6)
	Fe1–N3"	0.439	4.51	2.182	(5)		Fe1–O3'	0.303	3.59	2.253	(6)
	Fe1–N3'	0.432	4.33	2.193	(5)		Fe1–O3"	0.181	1.78	2.488	(6)

^aThe listed values are the density at the BCP, $\rho(r_c)$ in e Å⁻³; the Laplacian at the BCP, $\nabla^2\rho(r_c)$ in e Å⁻⁵; the internuclear distance, d_{Fe-X} , in Å.

^bNumbers concern to the six different types of metal–ligand interaction (see section 6 in the Results and Discussion).

information corresponding to the bond critical point (BCP) for the most stable complex. A local maximum in electron density corresponding to a BCP was located at each chemical bond in the molecules, and an additional critical points were found at the center of the ring formed by the central cation and the ligands.

The EDTA complex used as reference, which was the most stable of all examined, exhibited 6 BCP around the central cation; their $\rho(r_c)$ and $\nabla^2\rho(r_c)$ values fell in two groups, namely, 4 Fe–O BCP with $\nabla^2\rho(r_c)$ values from 9.93 to 10.83 e Å⁻⁵ and 2 Fe–N BCP with lower (3.66 e Å⁻⁵) $\nabla^2\rho(r_c)$ values. There were also 5 RCP that helped stabilize the complex because “a factor of great importance in the stability of a metal complex is the number of chelate rings formed in the resulting complex: the more the rings, the greater the stability of the complex”.⁹ Overall, the low ellipticity values found exclude an influence of π electrons on metal–ligand bonding in our complexes. As can be seen from Table 6 and Figure 6, $\rho(r_c)$ and $\nabla^2\rho(r_c)$, exhibited a similar pattern; thus, three pairs of metal–ligand binding were reflected in both $\rho(r_c)$ and $\nabla^2\rho(r_c)$ in all complexes.

AG-3s exhibited three imine interactions and three amine interactions in its metal–ligand bonding. The BCP for Fe–N (3, 3', 3'') (average 1.997 Å) and Fe–N (2, 2', 2'') (average

2.253 Å) were located midway between the two atoms. The density was low and the Laplacian positive at the BCP (Table 6), which is typical of many, if not all, transition metal complexes.⁶⁵ Three RCP were located at the center of the five-membered ring formed between the central cation and the ligands.

The BCPs of Fe–O and Fe–N in PM-3s were located midway between the atoms. Also, the density at the BCP was low and the Laplacian positive. This was also the case with previously studied, similar nickel complexes that exhibited comparable $\nabla^2\rho(r_c)$ values for their Fe–O bonds.⁶⁶ Figure 7 shows $\nabla^2\rho$ values for the Fe1–O2–N3''–O2''–N3', Fe1–N3–N3''–O2'–N3', and Fe1–O2–N3–O2''–O2' planes, which testify to the deformations in the charge concentrations on the lone electron pairs of the nitrogen atom by effect of its polarization toward the Fe atom. A total of three RCPs were located at the center of the six-membered ring formed between the central cation and the ligands.

The neutral complex AMD-3s was very similar to PM-3s as regards metal–ligand bonding. It also had an identical number of RCP stabilizing it; however, its rings were five- rather than six-membered. Also, the ρ and $\nabla^2\rho$ values for the 6 BCP around the iron atom were similar, and the Fe–O and Fe–N distances longer, than in PM-3s.

LR-3s contained a negatively charged tridentate ligand bonding to the metal via its carboxyl, ester, and pyridine groups. The structure was stabilized by 4 five-membered RCP, the $\nabla^2\rho$ values for the bonds of the ester and pyridine groups to the iron atom being identical and the values for the carboxyl bond coinciding with those for the same type of interaction (Table 6).

Finally, ASC-2s (the least stable chelate in the series) possessed a negatively charged ligand where the metal was bonded to the ligand via the O[−] ion and OH group.

As can be seen from Table 6 and Figure 8, our complexes exhibited six different types of metal–ligand interactions that were classified in terms Laplacian of the electron density values obtained from the QTAIM analysis, namely, (1) metal–ligand bonding via phenoxide anion group in the complexes

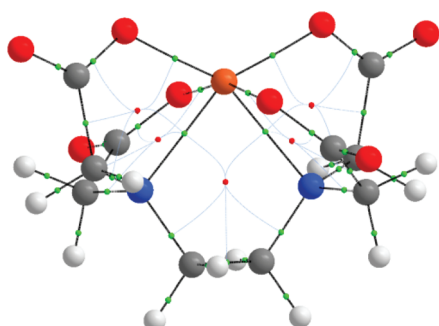


Figure 6. Molecular graph of the EDTA complex, showing the bond critical points, ring critical points, and paths connecting them.

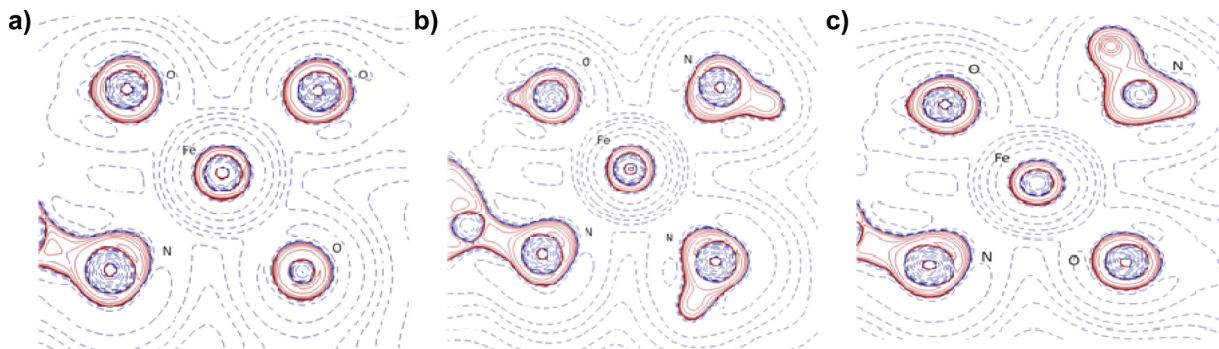


Figure 7. $\nabla^2\rho$ in the $\text{Fe}1-\text{O}2-\text{N}3''-\text{O}2''-\text{N}3'$ (A), $\text{Fe}1-\text{N}3-\text{N}3''-\text{O}2'-\text{N}3'$ (B), and $\text{Fe}1-\text{O}2-\text{N}3-\text{O}2''-\text{O}2'$ (C) planes. Positive values of $\nabla^2\rho$ are drawn by red and negatives by blue lines. Contours drawn at $0.000, \pm 2.0 \times 10^n, \pm 4.0 \times 10^n$, and $\pm 8.0 \times 10^n \text{ e } \text{\AA}^{-5}$, where $n = 0, \pm 1, \pm 2, \pm 3$.

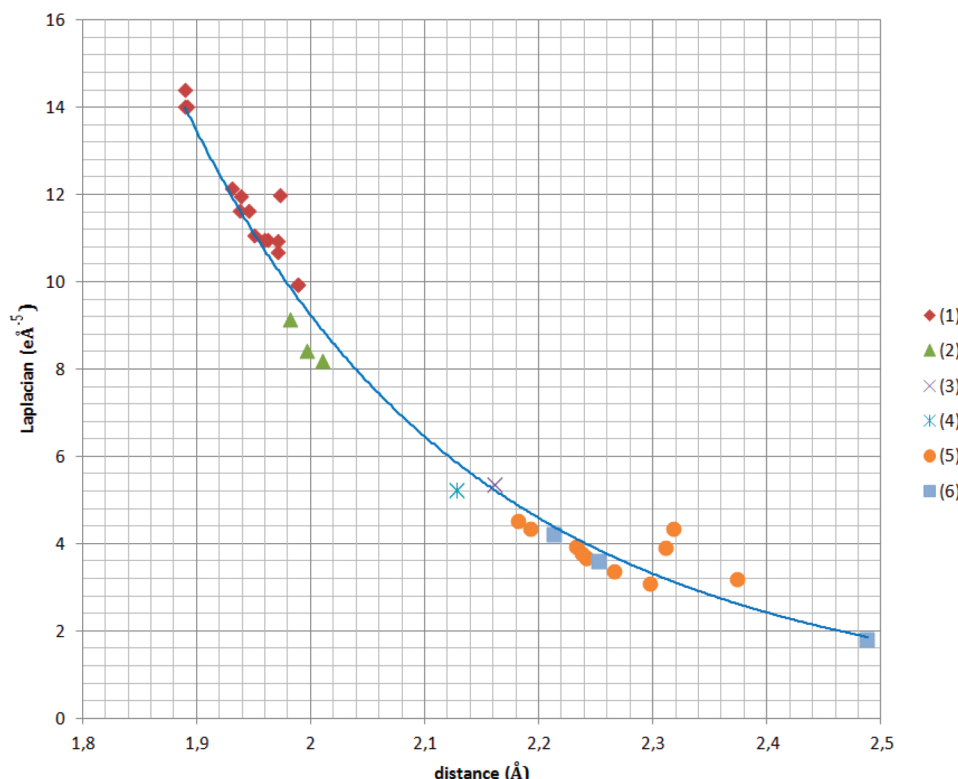


Figure 8. $\nabla^2\rho(r_c)$ ($\text{e } \text{\AA}^{-5}$) vs metal–ligand bond distances (\AA) for stable complexes studied. Six ranges of values are obtained depending on the different nature of metal–ligand bond. Red rhombic, green triangle, blue star, violet cross, orange circle, and blue square represent of 1, 2, 3, 4, 5, and 6 group in Table 6.

containing PM, AMD, ASC, or LR as ligand, the $\nabla^2\rho(r_c)$ values that ranged from 9.93 to $14.38 \text{ e } \text{\AA}^{-5}$ and corresponded to the shortest metal–ligand distances; (2) imine–metal bonding (AG-3s), with $\nabla^2\rho(r_c)$ of $8.41\text{--}9.14 \text{ e } \text{\AA}^{-5}$; (3) pyridine nitrogen–metal bonding (e.g., LR-3s), with $\nabla^2\rho(r_c)$ of $5.34\text{--}5.36 \text{ e } \text{\AA}^{-5}$; (4) ester–metal bonding (e.g., LR-3s), with $\nabla^2\rho(r_c)$ of $5.21\text{--}5.23 \text{ e } \text{\AA}^{-5}$; (5) bonding to primary, secondary, and tertiary amines, which spanned the $\nabla^2\rho(r_c)$ range $3.08\text{--}4.51 \text{ e } \text{\AA}^{-5}$ and included the complexes containing the ligands AMD, AG, PM, and EDTA; and (6) C–(HO)…Fe bonding, which was only found in ASC. Because differences in metal–ligand bonding strongly influence the stability of the formed complexes, we used QTAIM to expose them via the density and the Laplacian of the electron density. As can be seen from Table 6, the Laplacian decreased with increase in the Fe–ligand distance; therefore, the Laplacian of the electron density constitutes an effective indicator of metal–ligand binding

strength. This is quite apparent from Figure 8, which shows the Laplacian values obtained as a function of the metal–ligand bond distances in the compounds of Table 6.

7. Biological Implications. The oxidation of ascorbic acid and Amadori compounds is seemingly catalyzed by Fe(III) and Cu(II) ions, and potentially favored in individuals possessing relatively high blood levels of iron or copper by effect of some dysfunction.²¹

Aminoguanidine is known to inhibit the oxidation of ascorbic acid, but not that of Amadori compounds. Also, pyridoxamine is known to inhibit the oxidation of both ascorbic acid and Amadori compounds.^{19–21} These facts are seemingly difficult to explain if both oxidation processes are catalyzed by the same ion. Also, the theoretical and experimental exploration of new complexes intended to inhibit AGE formation^{19,23} revealed that LR-74 inhibits this process *in vitro* and also that it can interact directly with *reactive dicarbonyl species* such as glyoxal,

methylglyoxal, and glycoaldehyde.⁶⁷ In addition, LR-74 has been experimentally shown to form more stable Cu(II) complexes than pyridoxamine.¹⁹

We compared the stability (ΔG) of various iron complexes and found it to decrease in the following sequence: PM-3s (-158.2 kcal/mol) > AMD-3s (-126.1 kcal/mol) > AG-3s (-114.9 kcal/mol) > LR-3s (-104.3 kcal/mol) > ASC-2s (-77.0 kcal/mol). These results can be of help toward understanding the previous inconsistency. Thus, aminoguanidine, pyridoxamine, and LR-74 can inhibit the oxidation of ascorbic acid by chelating Fe(III) and suppressing its catalytic action as a result. The oxidation of the Amadori compound involves its previous chelation by Fe(III) and subsequent evolution to AGEs. On the basis of the previous ΔG values, aminoguanidine cannot compete with the Amadori compound for the chelation of iron; hence, it cannot inhibit the formation of AGEs. Also, on the basis of ΔG , pyridoxamine is a stronger chelating agent for Fe(III) than the Amadori compound. Consequently, pyridoxamine can inhibit or at least reduce the formation of AGEs more efficiently than the Amadori compound. Also, although LR-74 previously proved a stronger inhibitor than PM,¹⁹ this was not the case here; therefore, LR-74 must inhibit AGE formation via some of the above-described mechanisms (viz. carbonyl or radical scavenging) in addition to chelation.

ASSOCIATED CONTENT

Supporting Information

Distances from the Fe, N, and O atoms to the BCP ($d_{\text{Fe-BCP}}$, $d_{\text{BCP-X}}$), the three eigenvalues of the Hessian matrix (λ_1 , λ_2 , and λ_3), the ellipticity, and the $[\text{Fe}(\text{ASC})_2(\text{H}_2\text{O})_2]^+$ and $[\text{Fe}(\text{ASC})_3]$ structures. This material is available free of charge via the Internet at <http://pubs.acs.org>.

AUTHOR INFORMATION

Corresponding Author

*Phone: + 34 971 17 32 52. Fax: + 34 971 17 34 26. E-mail: dqufmi0@uib.es

Notes

The authors declare no competing financial interest.

ACKNOWLEDGMENTS

This work was funded by the Spanish Government via Project CTQ2008-02207/BQU. We thank the Supercomputational Centre of Catalunya (CESCA) and Supercomputational Center of Galicia (CESGA) for access to their computers facilities.

REFERENCES

- (1) Richardson, D. R.; Ponka, P. *Biochim. Biophys. Acta* **1997**, *1331*, 1.
- (2) Lieu, P. T.; Heiskala, M.; Peterson, P. A.; Yang, Y. *Mol. Aspects Med.* **2001**, *22*, 1.
- (3) Richardson, D. R. *Crit. Rev. Oncol. Hematol.* **2002**, *42*, 267.
- (4) Hahn, P.; Milam, A. H.; Dunaief, J. L. *Arch. Ophthalmol.* **2003**, *121*, 1099.
- (5) Smith, M. A.; Harris, P. L. R.; Sayre, L. M.; Perry, G. *Proc. Natl. Acad. Sci. U. S. A.* **1997**, *94*, 9866.
- (6) Lv, Z.; Jiang, H.; Xu, H.; Song, N.; Xie, J. *J. Neural Transm.* **2011**, *118*, 361.
- (7) Halliwell, B. *Biochem. Pharmacol.* **1995**, *49*, 1341.
- (8) Dickinson, P. J.; Carrington, A. L.; Frost, G. S.; Boulton, A. J. M. *Diabet. Metabol. Res. Rev.* **2002**, *18*, 260.
- (9) Crisponi, G.; Remelli, M. *Coord. Chem. Rev.* **2008**, *252*, 1225.
- (10) Kalinowski, D. S.; Richardson, D. R. *Pharmacol. Rev.* **2005**, *57*, 547.
- (11) Crichton, R. R.; Ward, R. J. *Curr. Med. Chem.* **2003**, *10*, 1051.
- (12) Labuza, T. P.; Reineccius, G. A.; O'Brien, J. In *Maillard Reactions in Chemistry, Food and Health*; Baynes, J. W. Eds.; Royal Society of Chemistry: Cambridge, U.K., 1994.
- (13) Brownlee, M. *Diabetis Care* **1992**, *15*, 1835.
- (14) Baynes, J. W.; Thorpe, S. R. *Diabetes* **1999**, *48*, 1.
- (15) Bailey, A. J.; Paul, R. G.; Knott, L. *Mech. Ageing Dev.* **1998**, *106*, 1.
- (16) Kume, S.; Takeya, M.; Mori, T.; Araki, N.; Suzuki, H.; Horiuchi, S.; Kodama, T.; Miyachi, Y.; Takahashi, K. *Am. J. Pathol.* **1995**, *147*, 654.
- (17) Hoyer, S. *J. J. Neural Transm.* **2002**, *109*, 341.
- (18) Adrover, M.; Vilanova, B.; Frau, J.; Muñoz, F.; Donoso, J. *Bioorg. Med. Chem.* **2008**, *16*, 5557.
- (19) Rahbar, S.; Figarola, J. L. *Arch. Biochem. Biophys.* **2003**, *419*, 63.
- (20) Voziany, P. A.; Hudson, B. G. *Ann. N. Y. Acad. Sci.* **2005**, *1043*, 807.
- (21) Monnier, V. M. *Arch. Biochem. Biophys.* **2003**, *419*, 1.
- (22) Ortega-Castro, J.; Adrover, J.; Frau, J.; Salvà, A.; Donoso, J.; Muñoz, F. *J. Phys. Chem. A* **2010**, *114*, 4634.
- (23) Ortega-Castro, J.; Adrover, M.; Frau, J.; Donoso, J.; Muñoz, F. *Chem. Phys. Lett.* **2009**, *475*, 277.
- (24) Ortega-Castro, J.; Adrover, M.; Frau, J.; Donoso, J.; Muñoz, F. *Chem. Phys. Lett.* **2008**, *465*, 120.
- (25) Lapouge, C.; Dangleterre, L.; Cornard, J.-P. *J. Phys. Chem. A* **2006**, *110*, 12494.
- (26) Amicangelo, J. C. *J. Chem. Theory. Comput.* **2007**, *3*, 2198.
- (27) Stoyanov, S. R.; Villegas, J. M.; Rillema, D. P. *Inorg. Chem.* **2003**, *42*, 7852.
- (28) Sousa, S. F.; Fernandes, P. A.; Ramos, M. J. *J. Phys. Chem. B* **2007**, *111*, 9146.
- (29) Strassner, T.; Taige, M. A. *J. Chem. Theory. Comput.* **2005**, *1*, 848.
- (30) Kakkar, R.; Dua, A.; Gahlot, P. *Polyhedron* **2007**, *26*, 5301.
- (31) Bader, R. F. W. *Atoms in molecules: A quantum theory*; Clarendon Press: Oxford, U.K., 1995.
- (32) Frisch, M. J.; Trucks, G. W.; Schlegel, H. B.; Scuseria, G. E.; Robb, M. A.; Cheeseman, J. R.; Scalmani, G.; Barone, V.; Mennucci, B.; Petersson, G. A.; Nakatsuji, H.; Caricato, M.; Li, X.; Hratchian, H. P.; Izmaylov, A. F.; Bloino, J.; Zheng, G.; Sonnenberg, J. L.; Hada, M.; Ehara, M.; Toyota, K.; Fukuda, R.; Hasegawa, J.; Ishida, M.; Nakajima, T.; Honda, Y.; Kitao, O.; Nakai, H.; Vreven, T.; Montgomery, J. A., Jr.; Peralta, J. E.; Ogliaro, F.; Bearpark, M.; Heyd, J. J.; Brothers, E.; Kudin, K. N.; Staroverov, V. N.; Kobayashi, R.; Normand, J.; Raghavachari, K.; Rendell, A.; Burant, J. C.; Iyengar, S. S.; Tomasi, J.; Cossi, M.; Rega, N.; Millam, N. J.; Klene, M.; Knox, J. E.; Cross, J. B.; Bakken, V.; Adamo, C.; Jaramillo, J.; Gomperts, R.; Stratmann, R. E.; Yazev, O.; Austin, A. J.; Cammi, R.; Pomelli, C.; Ochterski, J. W.; Martin, R. L.; Morokuma, K.; Zakrzewski, V. G.; Voth, G. A.; Salvador, P.; Dannenberg, J. J.; Dapprich, S.; Daniels, A. D.; Farkas, O.; Foresman, J. B.; Ortiz, J. V.; Cioslowski, J.; Fox, D. J. *Gaussian 09*, Revision A.1; Gaussian, Inc.: Wallingford, CT, 2009.
- (33) Zhao, Y.; Truhlar, D. G. *Theor. Chem. Acc.* **2008**, *120*, 215.
- (34) Zhao, Y.; Truhlar, D. G. *Acc. Chem. Res.* **2008**, *41*, 157.
- (35) Becke, A. D. *J. Chem. Phys.* **1994**, *98*, 10089.
- (36) Barone, V.; Cossi, M. *J. Phys. Chem. A* **1998**, *102*, 1995.
- (37) Cossi, M.; Rega, N.; Scalmani, G.; Barone, J. *J. Comput. Chem.* **2003**, *24*, 669.
- (38) Holleman, A. F.; Wiberg, E. In *Inorganic Chemistry*; Wiberg, N., Ed.; Academic Press: New York, 2001.
- (39) CCDC 2011 (version 5.32), <http://www.ccdc.cam.ac.uk>.
- (40) Smith, D. M. A.; Dupuis, M.; Vorpagel, E. R.; Straatsma, T. P. *J. Am. Chem. Soc.* **2003**, *125*, 2711.
- (41) Keith, T. A. AIMAll (version 10.10.11 professional), <http://aim.tkgristmill.com>.
- (42) Liebre, E.; Smith, G. B. L. *Chem. Rev.* **1939**, *25*, 213.
- (43) Saveleva, V. V.; Lavrenova, L. G. *Russ. J. Inorg. Chem.* **1998**, *43*, 302.

- (44) Aitken, D. J.; Albinati, A.; Gautier, A.; Husson, H.-P.; Morgant, G.; Nguyen-Huy, D.; Kozelka, J.; Lemoine, P.; Ongeri, S.; Rizzato, S.; Viossat, B. *Eur. J. Inorg. Chem.* **2007**, 3327.
- (45) Zubkov, S. V.; Seifullina, I. I.; Feldman, S. V. *J. Coord. Chem.* **1996**, 22, 181.
- (46) Romanenko, G. V.; Podberezska, N. V. *J. Struct. Chem.* **1992**, 33, 141.
- (47) Meier, R.; Heinemann, F. W. *Inorg. Chim. Acta* **2002**, 337, 317.
- (48) Allen, F. H. *Acta Crystallogr. B* **2002**, 58, 380.
- (49) Yemeli Tido, E. W.; Alberda van Ekenstein, G. O. R.; Meetsma, A.; van Koningsbruggen, P. J. *Inorg. Chem.* **2008**, 47, 143.
- (50) Hayami, S.; Miyazaki, S.; Yamamoto, M.; Hiki, K.; Motokawa, N.; Shuto, A.; Inoue, K.; Shinmyozu, T.; Maeda, Y. *Bull. Chem. Soc. Jpn.* **2006**, 79, 442.
- (51) Franklin, K. J.; Richardson, M. F. *Inorg. Chem.* **1980**, 19, 2107.
- (52) Zhang, S. H.; Jiang, Y. M.; Zhou, Z. Y. *Chin. J. Chem.* **2004**, 22, 1303.
- (53) Leovac, V. M.; Joksovic, M. D.; Divjakovic, V.; Jovanovic, L. S.; Saranovic, Z.; Pevec, A. *J. Inorg. Biochem.* **2007**, 101, 1094.
- (54) Franklin, K. J.; Richardson, M. F. *Chem. Commun.* **1978**, 97.
- (55) Adrover, M.; Vilanova, B.; Frau, J.; Muñoz, F.; Donoso, J. *Bioorg. Med. Chem.* **2008**, 16, 5557.
- (56) Chen, J.; Pill, T.; Beck, W. Z. *Naturforsch. B* **1989**, 44, 459.
- (57) Tonkovic, M.; Jakas, A.; Horvat, S. *Biometals* **1997**, 9, 55.
- (58) Seib, P. A.; Tolbert, B. M. *Ascorbic acid: Chemistry, Metabolism and Uses; Advances in Chemistry series 200*; America Chemical Society: Washington, DC, 1989.
- (59) Unaleroğlu, C.; Mert, Y.; Zumreoglu-Karan, B. *Synth. React. Inorg. Met. Org. Chem.* **2001**, 31, 1531.
- (60) Scarpa, M.; Stevanato, R.; Viglino, P.; Rigo, A. *J. Biol. Chem.* **1983**, 258, 6695.
- (61) Buettner, G. *Free Radical Res. Commun.* **1986**, 1, 349.
- (62) Scarpa, M.; Vianello, F.; Signor, L.; Zennaro, L.; Rigo, A. *Inorg. Chem.* **1996**, 35, 5201.
- (63) Jameson, R. F.; Blackburn, N. J. *J. Chem. Soc., Dalton Trans.* **1982**, 9.
- (64) Tajmir-Riahi, H. A. *J. Inorg. Chem.* **1991**, 42, 47.
- (65) Koritsanszky, T. S.; Coppens, P. *Chem. Rev.* **2001**, 101, 1583.
- (66) Smith, G. T.; Mallinson, P. R.; Frampton, C. S.; Farrugia, L. J.; Peacock, R. D.; Howard, J. A. K. *J. Am. Chem. Soc.* **1997**, 119, 5028.
- (67) Peyroux, J.; Sternberg, M. *Pat. Biol.* **2006**, 54, 405.